

Multifunctional icariin and tanshinone IIA co-delivery liposomes with potential application for Alzheimer's disease

Jiao Wang^{a,b}, Liang Kong^{a,c}, Rui-Bo Guo^a, Si-Yu He^a, Xin-Ze Liu^a, Lu Zhang^a, Yang Liu^a, Yang Yu^a, Xue-Tao Li^a and Lan Cheng^a

^aSchool of Pharmacy, Liaoning University of Traditional Chinese Medicine, Dalian, China; ^bShenyang Medical College, Shenyang, China; ^cKey Laboratory of Ministry of Education for TCM Viscera-State Theory and Applications, Liaoning University of Traditional Chinese Medicine, Shenyang, China

ABSTRACT

The blood–brain barrier (BBB) is a protective barrier for brain safety, but it is also a major obstacle to the delivery of drugs to the cerebral parenchyma such as the hippocampus, hindering the treatment of central nervous system diseases such as Alzheimer's disease (AD). In this work, an anti-AD brain-targeted nanodrug delivery system by co-loading icariin (ICA) and tanshinone IIA (TSIIA) into Aniopep-2-modified long-circulating (Ang2-ICA/TSIIA) liposomes was developed. Low-density lipoprotein receptor-related protein-1 (LRP1) was a receptor overexpressed on the BBB. Angiopep-2, a specific ligand of LRP1, exhibited a high binding efficiency with LRP1. Additionally, ICA and TSIIA, drugs with neuroprotective effects are loaded into the liposomes, so that the liposomes not only have an effective BBB penetration effect, but also have a potential anti-AD effect. The prepared Ang2-ICA/TSIIA liposomes appeared narrow dispersity and good stability with a diameter of 110 nm, and a round morphology. Cell uptake observations, BBB models *in vitro*, and imaging analysis *in vivo* showed that Ang2-ICA/TSIIA liposomes not only penetrate the BBB through endocytosis, but also accumulate in N2a cells or brain tissue. The pharmacodynamic analysis *in vivo* demonstrated that Ang2-ICA/TSIIA liposomes could improve AD-like pathological features in APP/PS1 mice, including inhibiting neuroinflammation and oxidative stress, reducing apoptosis, protecting neurons, and improving cognitive function. Therefore, Ang2-ICA/TSIIA liposomes are considered a potentially effective therapeutic strategy for AD.

ARTICLE HISTORY

Received 21 March 2022
Revised 25 April 2022
Accepted 25 April 2022

KEYWORDS

Angiopep-2; icariin; tanshinone IIA; liposomes; Alzheimer's disease


1. Introduction

Alzheimer's disease (AD) is one of the most common types of dementia in the elderly, which is characterized by a large number of extracellular senile plaques composed of β -amyloid peptide (A β) deposits, intracellular neurofibrillary tangles consisting of hyperphosphorylated tau proteins, neuroinflammation, oxidative stress, and a selective loss of neurons in neuropathology, which eventually lead to cognitive dysfunction in patients (Eratne et al., 2018). Since the number of AD patients is greatly increasing, and available therapies such as cholinesterase inhibitors, NMDA receptor antagonists, etc. can only provide short-term symptom relief, and have little effect on the improvement of patients with moderate to severe AD, the need for effective drug therapy is becoming more and more obvious (Kong et al., 2020). Several hypotheses have been proposed about the pathogenesis of the disease, including the A β hypothesis, the neuroinflammation hypothesis, the Tau protein hypothesis, etc., but in the past decade, potential therapeutic drugs developed against these hypotheses have mostly failed in most clinical trials, mainly

due to the drugs were restricted by the blood–brain barrier (BBB), only <2% of them could reach their target (Formicola et al., 2019). The major obstacle encountered in the effective treatment of Alzheimer's and other central nervous system diseases is BBB, preventing most drugs, peptides and large molecules across the endothelial cell lining to protect the brain from its adverse side effects (Poovaiah et al., 2018). Researchers around the world are trying to make attempts to formulate a drug molecule and delivery system that can able to deliver drugs to the brain by crossing the BBB and maintain the higher concentrations in the brain (Baranowska-Wójcik & Sz wajgier, 2020). The development of nanomedicine technology offers potential to overcome this problem (Gao, 2016). In this field, liposomes, a new type of nano drug delivery system, have a good application prospect because of their unique capability to target BBB (Ross et al., 2018).

Liposomes are non-degradable, nontoxic and non-immune *in vivo*. As a drug carrier, liposomes are able to improve the therapeutic effect, reduce drug toxicity, reduce drug dose, etc., and can be used as an ideal carrier to improve the concentration of drugs in the brain. Liposomes with particle size

CONTACT Xue-Tao Li  lixuetao1979@163.com; Lan Cheng  sychenglan@163.com  School of Pharmacy, Liaoning University of Traditional Chinese Medicine, Dalian 116600, China

 Supplemental data for this article can be accessed [here](#).

© 2022 The Author(s). Published by Informa UK Limited, trading as Taylor & Francis Group.

This is an Open Access article distributed under the terms of the Creative Commons Attribution-NonCommercial License (<http://creativecommons.org/licenses/by-nc/4.0/>), which permits unrestricted non-commercial use, distribution, and reproduction in any medium, provided the original work is properly cited.

ranging from 20 nm to 1000 nm can be used as carriers of hydrophobic, hydrophilic, and amphiphilic drugs. Liposomes are highly lipophilic and can be transported into the brain by passive transport, membrane fusion with cerebrovascular endothelial membranes, or by endocytosis (Carita et al., 2018; Shah et al., 2020). In addition, specific targeting of liposomes can be achieved by modifying appropriate targeting vectors. Liposomes modified with specific ligands or antibodies can realize active brain targeting by recognizing endogenous receptors on cerebrovascular endothelial membranes (Ruan et al., 2021). Angiopep-2 is composed of 19 amino acids, whose amino acid sequence is TFFYGGSRGKRNNFKTEEY and molecular weight is 2.4 kDa (Wang et al., 2018). Angiopep-2 is a family of peptides that can target the low-density lipoprotein receptor-related protein (LRP) domain and have a good ability of assisting carriers to penetrate BBB (Zhu et al., 2021). It has been proven that Angiopep-2 binds to nanocarriers to promote specific penetration of drug delivery or genes through low-density lipoprotein receptor-related protein-1 (LRP1) receptor-mediated endocytosis of the BBB, thus improving the therapeutic effect of central nervous system diseases such as AD (Candela et al., 2015; Duro-Castano et al., 2021).

Icariin (ICA, $C_{33}H_{40}O_{15}$, molecular weight 676.67) the main component from traditional Chinese herb *Epimedium brevicornu Maxim.*, has a wide range of pharmacological effects, such as anti-osteoporotic, antidepressant, and estrogen-like pharmacological activities (Zu et al., 2019; He et al., 2020; Zhou et al., 2020). In addition to that, ICA also can rescue major AD hallmarks in AD, including (i) that it improved the cognitive function of APP/PS1 mice via regulating brain metabolism, mitochondrial functions (Chen et al., 2016); (ii) that it promoted the survival, proliferation, and differentiation of neural stem cells in AD model (Ma et al., 2021); (iii) that it attenuated synaptic and cognitive deficits by $A\beta_{1-42}$ *in vivo* (Sheng et al., 2017); (iv) that it decreased both APP and $A\beta$ levels and increases neurogenesis to improve cognitive function of Tg2576 mice, etc. (Li et al., 2015). Tanshinone IIA (TSIIA, $C_{19}H_{18}O_3$, molecular weight 294.34) is an active component extracted from *Salvia miltiorrhiza Bunge* and exerts multiple neuroprotective potentials relevant to AD, including (i) that it decreased the levels of inflammation induced by $A\beta_{1-42}$ in brain tissues of AD model rats (Lu et al., 2016); (ii) that it played a protective role of mesenchymal stem cells against neuroinflammation induced by $A\beta_{25-35}$ (Huang et al., 2019); (iii) that it degraded endogenous Tau proteins and inhibited Tau fibrillation through the ubiquitin–proteasome pathway (Cai et al., 2020); (iv) that it attenuated $A\beta$ -induced neurotoxicity by down-regulating COX-2 expression and PGE2 synthesis via inactivation of NF- κ B pathway in SH-SY5Y cells, etc. (Geng et al., 2019).

Based on the above previous studies, ICA and TSIIA have been confirmed to have a certain effect on alleviating AD-like pathological features, and are potential anti-AD drugs. At present, there are certain limitations in oral administration, such as poor water solubility, the first-pass effect, low bio-availability, etc., which limit the clinical application of ICA and TSIIA. In this study, we prepared ICA and TSIIA

co-delivery liposomes using thin film dispersion and modified Ang2 on the liposome surface to help them cross BBB. We aimed to evaluate the brain targeting ability of Ang2 modified ICA and TSIIA co-delivery liposomes and its therapeutic effect on APP/PS1 mice.

2. Materials and methods

2.1. Materials, cells, and animals

Egg yolk phosphatidylcholine (EPC) and cholesterol (Chol) were obtained from the Avanti Polar Lipids, Inc. (purity >99%, Alabaster, AL). Polyethylene glycol-distearoyl phosphatidylethanolamine (DSPE-PEG₂₀₀₀) and polyethylene glycol-distearoyl phosphatidylethanolamine-Angiopep-2 (DSPE-PEG₂₀₀₀-Ang2) were purchased from the Xi'an ruixi Biological Technology Co., Ltd. (Xi'an, China). Icariin and TSIIA were purchased from the Chengdu Pufei De Biotech Co., Ltd. (purity > 99.8%, Chengdu, China). Coumarin-6 (Cou-6) and 1,1-dioctadecyl-3,3,3,3-tetramethylindotricarbocyanineiodide (DiR) were obtained from the Sigma-Aldrich (St. Louis, MO). 4',6-Diamidino-2-phenylindole (DAPI) was purchased from the Beijing biyuntian Technology Co., Ltd. (Beijing, China). HE and Nissl staining kits were purchased by Dalian Meilun Biotechnology Co., Ltd. (Dalian, China). Enzyme-linked immunosorbent assay (ELISA) kits (including interleukin-6 (IL-6), IL-1 β , and tumor necrosis factor- α (TNF- α)) were supplied by Beijing Solarbio Biotech Co., Ltd. (Beijing, China). Total superoxide dismutase (SOD), malondialdehyde (MDA), and glutathione peroxidase (GSH-Px) kits were ordered from Nanjing Jiancheng Bioengineering Institute (Nanjing, China). Bax, Bcl-2, caspase-3, GFAP, and GAPDH antibodies and horseradish peroxidase (HRP) biotin labeled secondary antibody were purchased from Biosynthesis Biological Co., Ltd. (Beijing, China). $A\beta_{1-42}$ and SYN antibodies were ordered from Abcam Co., Ltd. (Cambridge, MA). Iba-1 antibody was provided by FUJIFILM Wako Pure Chemical Corporation (Osaka, Japan). Fluorescein isothiocyanate (FITC)- or Cy3-conjugated secondary antibodies were purchased from Jackson ImmunoResearch Lab (West Grove, PA). All other reagents used were of analytical grade. Mouse brain microvascular endothelial cell line (bEnd.3) and mouse brain neuroma cell line (N2a) were purchased from iCell Bioscience Inc. (Shanghai, China). The cells were cultured in incubators maintained at 37 °C with 95% air and 5% CO₂ under fully humidified conditions. The medium composition of bEnd.3 cells and N2a cells included Dulbecco's modified Eagle's medium (DMEM) (EallBio, Beijing, China), 10% fetal bovine serum (FBS) (EallBio, Beijing, China), and 1% penicillin–streptomycin solution (Meilun, Dalian, China). All experiments were performed on cells in the logarithmic growth phase. Seven-month-old APP/PS-1 double transgenic (Tg) mice were purchased from Beijing Huafukang Biological Co., Ltd. (Beijing, China). The same age C57BL/6 mice were provided by Liaoning Changsheng Biological Co., Ltd. (Benxi, China). All procedures were performed according to the guidelines of Liaoning University of Traditional Chinese Medicine Institutional Animal Care and Use Committee. All mice for experiments were group-housed with comfortable

environment ($65 \pm 5\%$ humidity, $25 \pm 2^\circ\text{C}$ temperature, and 12 h light/dark cycle illumination).

2.2. Liposomes preparation

Three types of liposomes, blank control liposomes, ICA and TSIIA co-delivery liposomes (ICA/TSIIA liposomes), ICA and TSIIA co-delivery liposomes modified with angiopep-2 (Ang2-ICA/TSIIA liposomes), were prepared. These liposomes were prepared using the thin-film hydration method (Zheng et al., 2015). Briefly, EPC, Chol, DSPE-PEG₂₀₀₀, ICA, TSIIA, and DSPE-PEG₂₀₀₀-Ang2 (26.18:1:0.069:0.071:0.164:0.038, molar ratio) were first dissolved in chloroform, and followed by evaporating under negative pressure to form liposome suspensions using a rotary evaporator (RE-52C, Shanghai Yaguang Instrument Co., Ltd., Shanghai, China) at 40°C to obtain a thin film. The thin film was hydrated with 5 mL of Tris base solution ($\text{pH} = 10.0$) via sonication in a water bath, and then the suspension was sonicated at 200 W for 10 min via probe sonicator (JY92-IIN, Xinzhi Biotechnology Co., Ltd., Ningbo, China). Subsequently, the sample was extruded three times by a polycarbonate membrane with $0.22\ \mu\text{m}$ wells, thus completing the preparation of Ang2-ICA/TSIIA liposomes. ICA/TSIIA liposomes and blank control liposomes were prepared by the same method as described above without the addition of DSPE-PEG₂₀₀₀-Ang2 or ICA, TSIIA. To investigate cell uptake and brain targeting, Cou-6 and DiR liposomes were also prepared using the same method, but the drug was replaced with a fluorescent probe (EPC: Cou-6 = 12:1, molar ratio; EPC: DiR = 13:1, molar ratio).

2.3. Characterization of liposomes

The morphological characteristics of liposomes were observed by transmission electron microscopy (TEM, JEM-1200EX; JEOL, Tokyo, Japan). Liposomes were diluted to a suitable concentration, stained with 2% phosphotungstic acid, dried and observed by TEM and they were dripped on mica sheets, dried naturally and then observed by AFM. The particle size, polydispersity index (PDI), and zeta potential of liposomes were measured by Zetasizer Zano ZS (Litesizer 500; Anton Paar Instruments Ltd., Graz, Austria). Encapsulation efficiency (EE) was determined using a previously reported method. Five hundred microliters of liposome dispersions was eluted with PBS ($\text{pH} = 7.4$) through a Sephadex G-50 column to remove unloaded drugs. The entrapped drugs were determined by disrupting the liposome dispersions with methyl alcohol. Drugs in liposomes were measured by high-performance liquid chromatography (HPLC, Agrest 1100; Elite Analytical Instrument Co., Ltd., Dalian, China). The EE of drugs was calculated as $\text{EE}\% = (W_{\text{encapsulated}}/W_{\text{total}}) \times 100\%$, where $W_{\text{encapsulated}}$ and W_{total} represent the amount of drugs in the liposomes and the total amount of drugs, respectively. The drug loading (DL%) of liposomes was calculated using the following equation: $\text{DL}\% = (W_{\text{loaded drug}}/W_{\text{Total amount of lipids}}) \times 100\%$ (Yu et al., 2022). Ang2-ICA/TSIIA liposomes were stored at 4°C , and the particle size, EE%, and leakage rate (LR) were investigated at

0, 10, 20, and 30 days, respectively. The LR were calculated as $\text{LR}\% = (\text{EE}_1 - \text{EE}_2)/\text{EE}_1 \times 100\%$, where EE_1 and EE_2 represent the EE% at 0 day, EE% at 10, 20, or 30 days, respectively. Each experiment was repeated in triplicate.

2.4. Cellular uptake

The cell uptake of Cou-6 liposomes and Ang2-Cou-6 liposomes in bEnd.3 cells was analyzed by fluorescence microscopy (Nikon Ti-S, Tokyo, Japan). The bEnd.3 cells were grown on six-well plates at a density of 4×10^5 cells/well. To examine dose dependence, Cou-6 liposomes and Ang2-Cou-6 liposomes at concentrations of 1.5, 3, and $6\ \mu\text{M}$ of Cou-6 were added for 2 h, and blank control liposomes were used as blank controls. Then, cells treated with Cou-6 liposomes and Ang2-Cou-6 liposomes were incubated for different amounts of time (1, 2, and 4 h). The final concentration of Cou-6 was $3\ \mu\text{M}$. Subsequently, cells were washed with PBS to remove excess Cou-6, fixed with 4% paraformaldehyde for 30 min at room temperature (RT), and the nuclei were then stained with DAPI (1:50, v/v) for 10 min in a dark room. Finally, fluorescence images of the bEnd.3 cells were observed by a fluorescence microscope. The cellular uptake of Cou-6 liposomes and Ang2-Cou-6 liposomes in bEnd.3 cells was further verified using flow cytometry (BD Biosciences, Franklin Lakes, NJ). The method is the same as described above. Finally, the cells were washed with PBS and trypsinized with 0.25% trypsin, harvested, and centrifuged at 1500 rpm for 3 min. Cells were resuspended in $400\ \mu\text{L}$ PBS, and the fluorescence intensity of the samples was quantified by flow cytometry (BD Biosciences, Franklin Lakes, NJ).

2.5. Transport of liposomes across BBB models

To evaluate the transport of liposomes across BBB model *in vitro*, the model was constructed by placing the co-culture (bEnd.3 and N2a cells) was constructed according to previously published reports (Dos Santos Rodrigues et al., 2020). Briefly, the co-culture barrier was formed by seeding bEnd.3 cells (5×10^5 cells/well) and N2a cells (4×10^5 cells/well) on luminal side and abluminal side of the insert, respectively. The media of barrier was replaced with fresh media every two days and cells were checked for confluency according to the previously reported. Cou-6 liposomes and Ang2-Cou-6 liposomes solution (the final concentration of Cou-6 was $3\ \mu\text{M}$) in $500\ \mu\text{L}$ of fresh serum containing buffer were added in the upper compartment of the co-culture barrier insert for 4 h. Then, N2a cells were treated as described above and the cells was analyzed as the same way described in the cellular uptake study using fluorescence microscopy and flow cytometry.

2.6. Imaging in APP/PS-1 mice

APP/PS-1 mice were used to evaluate the distribution of liposomes modified with Ang2 *in vivo*. First, DiR liposomes and Ang2-modified DiR ($2\ \mu\text{g}$ DiR/mouse) were injected through the tail vein ($n = 3$). The mice were anesthetized with

isoflurane, and fluorescence images and normal images of the mice were captured at 0, 6, 12, and 24 h using an *in vivo* fluorescence imaging system (Carestream, FX Pro, Woodbridge, CT). Subsequently, the mice were sacrificed at 24 h, the brain, hearts, livers, spleens, lungs, and kidneys were dissected for *ex vivo* fluorescence imaging using a fluorescence imaging system.

2.7. Evaluation of anti-AD effect *in vivo*

The experiments were carried out in 7-month-old APP/PS1 mice and wild-type (WT) littermates of the same age on a C57/Bl6J genetic background. Twenty-four APP/PS-1 mice were randomly divided into four groups, all mice were separated into four groups ($n=6$), namely the control group, model group, free ICA/TSIIA group, ICA/TSIIA liposomes group, and Ang2-ICA/TSIIA liposomes group, and WT littermates served as normal control. APP/PS-1 mice were intraperitoneally injected with saline, ICA/TSIIA solution, ICA/TSIIA liposomes or Ang2-ICA/TSIIA liposomes (both ICA and TSIIA were 10 mg/kg/day), for 40 days. The mice in the control group were also treated with saline for 40 days. On the 40th day of treatment, the mice were sacrificed to evaluate the improvement effect of various formulations on the pathological features of AD, including, the cognitive function of mice was analyzed through Morris water maze (MWM) and nest building experiments. The cortical and hippocampal neuron structures were observed by HE and Nissl staining. IL-6, TNF- α , and IL-1 β expression levels were analyzed to evaluate neuroinflammation. SOD and GSH-Px activities, MDA content were quantified to evaluate oxidative stress. The expression levels of Bax, Bcl-2, caspase-3, Iba-1, and GFAP were observed by immunohistochemical staining after treatment with various formulations. In addition, the expression level of A β ₁₋₄₂ protein was detected by immunohistochemical staining and Western blot. Detailed methods are described in [Supplementary methods](#).

2.8. Statistical analysis

Data were expressed as mean \pm standard error of the mean (SEM), and analyzed by GraphPad Prism 9.0 software (La Jolla, CA). Differences between groups were assessed by one-way analysis of variance (ANOVA). Post hoc multiple comparisons were performed with the Student–Newman–Keuls test. Escape latency data were subjected to repeated-measures two-way ANOVA followed by Bonferroni's post hoc test. $p < .05$ was considered as significant difference.

3. Results and discussion

3.1. Characterization of the liposomes

The encapsulation efficiencies of ICA and TSIIA were (89.98 \pm 2.66)%, (91.46 \pm 4.97)% for ICA/TSIIA liposomes and (89.92 \pm 3.51)%, (92.45 \pm 3.20)% for Ang2-ICA/TSIIA liposomes, respectively. The DL% capacities of these liposomes were

found to be 3.33% and 3.26%, respectively. As depicted in [Figure 1\(A\)](#), the image analysis performed using TEM showed shape, morphology, and uniform distribution of Ang2-ICA/TSIIA liposomes. Physical properties including particle size, zeta potential, and PDI, are shown in [Figure 1\(B–E\)](#). The particle sizes of the blank control liposomes, ICA/TSIIA liposomes, and Ang2-ICA/TSIIA liposomes were (85.94 \pm 1.51), (92.79 \pm 3.11), and (111.26 \pm 11.65) nm, respectively, the PDI of them was (0.21 \pm 0.01), (0.23 \pm 0.02), and (0.24 \pm 0.03), respectively, with a narrow PDI (≤ 0.25) and a normal distribution, indicating that the particle size distribution of liposomes is uniform, and the surface modification of liposomes did significantly increase the particle size of the liposomes. In addition, the zeta potential of the blank control liposomes, ICA/TSIIA liposomes, and Ang2-ICA/TSIIA liposomes was found to be $-$ (0.40 \pm 0.10), $-$ (0.70 \pm 0.10), and $-$ (1.53 \pm 0.38) mV, respectively. Due to the presence of EPC, liposomes showed a slightly negative charge. Moreover, Ang2-ICA/TSIIA liposomes were placed at 4 $^{\circ}$ C for 30 d to check their storage stability. The changes in the EE and LR of the drugs are shown in [Table 1](#), and the EE of both ICA and TSIIA is slightly reduced, but above 70%. In addition, as shown in [Figure 1\(F,G\)](#), the particle size, PDI of the Ang2-ICA/TSIIA liposomes changed also within a reasonable range after storage for 30 days at 4 $^{\circ}$ C, indicating that the liposomes had improved stability. This may be because the PEGylation of liposomes improves their stability, increases their residence time as well as their accumulation in the brain by forming a hydrophilic layer on liposomes (Endo-Takahashi et al., 2021). PEGylation and a slightly negative charge of liposomes also prevent macrophages from clearing liposomes. However, the PEG chains can hinder the binding and internalization of liposomes to neural cells, however, this can be overcome by coupling ligands to the distal end of PEG chains, thus maintaining long circulation properties (Chen et al., 2017; Lakkadwala et al., 2019).

3.2. Cellular uptake and targeting effects *in vitro*

In order to observe and analyze the active uptake of liposomes by nerve cells, ICA and TSIIA were replaced by Cou-6 fluorescent dye, which is often used to investigate the intracellular uptake and distribution of liposome carriers (Yu et al., 2012). bEnd.3 cells, a type of mouse brain microvascular endothelial cell line, were used as a cell model to evaluate whether Ang2-modified liposomes delivered more drugs to cells than other groups of liposomal formulations. Intracellular distribution of Cou-6 liposomes and Ang2-Cou-6 labeled liposomes was observed by fluorescence microscopy. The nuclei were stained with DAPI (blue) and Cou-6 was green. [Figure 2\(A,B\)](#) shows the intracellular distribution of Cou-6 liposomes with final concentrations of 1.5, 3, and 6 μ M of Cou-6. The results showed that intracellular distribution of Cou-6 liposomes and Ang2-Cou-6 liposomes gradually increased with the increasing final concentration of Cou-6 ($p < .05$). [Figure 2\(C,D\)](#) reveals that intracellular distribution of Cou-6 and Ang2-Cou-6 liposomes gradually increased with incubation time. Moreover, Ang2-Cou-6 exhibited the most

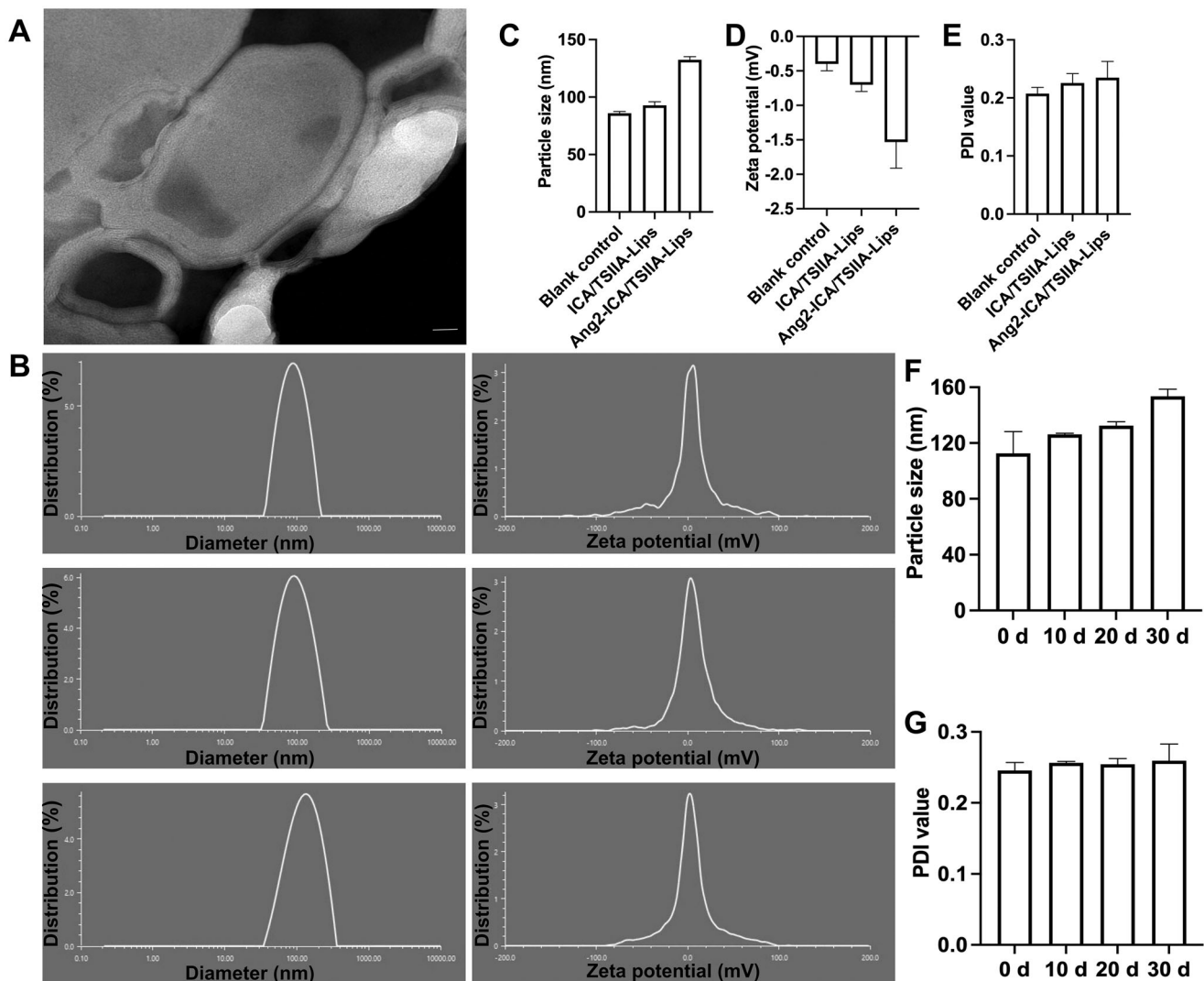


Figure 1. Characterization of Ang2-ICA/TSIIA liposomes. (A) TEM image of Ang2-ICA/TSIIA liposomes, scale bar = 20 nm; (B) representative images of particle sizes and zeta potential of the varying liposomal formulations; (C) quantitative analysis of particle size of liposomes; (D) quantitative analysis of zeta potential of liposomes; (E) quantitative analysis of PDI value of liposomes; (F, G) quantitative analysis of Ang2-ICA/TSIIA liposomes particle size (F) and PDI value (G) change at 4 °C for 30 days. All data are presented as mean \pm SD ($n = 3$).

Table 1. Encapsulation efficiency and leakage rate of the varying liposomes ($n = 3$).

Liposomes	Drugs	0 d		10 d		20 d		30 d	
		EE%	LR%	EE%	LR%	EE%	LR%	EE%	LR%
ICA/TSIIA liposomes	ICA	94.84 \pm 0.59	0	93.96 \pm 0.44	0.92 \pm 0.21	89.82 \pm 3.36	5.286 \pm 4.00	79.64 \pm 4.56	16.04 \pm 4.33
	TSIIA	89.96 \pm 1.25	0	82.58 \pm 2.74	8.21 \pm 2.65	82.48 \pm 4.41	8.27 \pm 5.88	79.45 \pm 2.26	11.65 \pm 3.50
Ang2-ICA/TSIIA liposomes	ICA	97.09 \pm 1.15	0	91.24 \pm 1.63	6.03 \pm 1.18	84.56 \pm 7.25	12.87 \pm 8.08	73.40 \pm 3.43	24.41 \pm 2.96
	TSIIA	93.52 \pm 2.24	0	91.68 \pm 3.62	1.95 \pm 3.97	86.97 \pm 4.05	6.99 \pm 4.35	77.85 \pm 5.40	16.64 \pm 7.65

robust green fluorescence, suggesting the most efficient cell internalization at the same concentration or the same incubation time ($p < .05$).

To quantitatively analyze changes in cell uptake of a various of liposomal formulations, intracellular fluorescence intensity was analyzed by flow cytometry. The results of flow cytometry were in good agreement with those obtained by fluorescence microscopy. Results as shown in Figure 2(E,F), after incubation with liposomes containing a various of concentrations of Cou-6, the fluorescence intensity of cells was concentration-dependent, the fluorescence intensity was in

the order of 6 μ M > 3 μ M > 1.5 μ M ($p < .05$). At each concentration, the fluorescence intensity of Ang-Cou-6 liposomes group was significantly stronger than that of Cou-6 liposomes group ($p < .05$). In addition, with the extension of incubation time, the fluorescence intensity of both Cou-6 and Ang-Cou-6 liposomes was significantly increased. The fluorescence intensity was in the order of 4h > 2h > 1h ($p < .05$). Similarly, the fluorescence intensity of Ang-Cou-6 liposomes was significantly stronger than that of Cou-6 liposomes (Figure 2(G,H), $p < .05$). All the results indicate that drug accumulation in the Ang2-Cou-6 liposomes was the

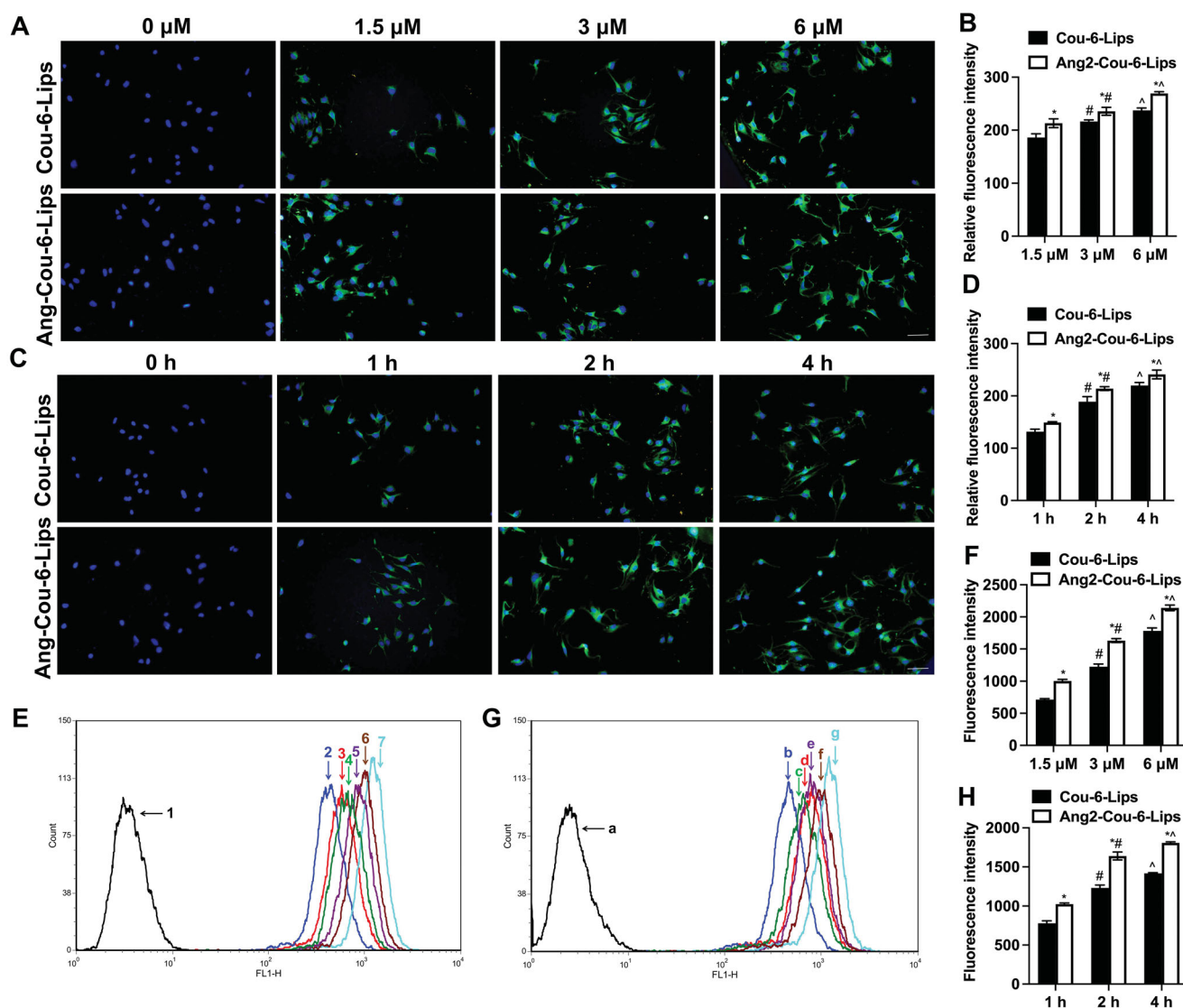


Figure 2. Intracellular distribution and uptake after incubation with varying formulations. (A) Cellular uptake and distribution of bEnd.3 cells treated with Cou-6 liposomes and Ang2-Cou-6 liposomes at a series of concentrations of Cou-6, scale bar = 50 μm; (B) semi-quantitative analysis of relative fluorescence intensity. *, vs. Cou-6 liposomes; #, vs. 1.5 μM; ^, vs. 3 μM. $p < .05$; (C) cellular uptake and distribution of bEnd.3 cells treated with Cou-6 liposomes and Ang2-Cou-6 liposomes at a series of time points, scale bar = 50 μm; (D) semi-quantitative analysis of relative fluorescence intensity. *, vs. Cou-6 liposomes; #, vs. 1 h; ^, vs. 2 h. $p < .05$; (E) analysis of cellular uptake of bEnd.3 cells treated with Cou-6 liposomes and Ang2-Cou-6 liposomes at a series of concentrations of Cou-6 by flow cytometry; (1) blank control, (2) Cou-6 liposomes (1.5 μM), (3) Ang2-Cou-6 liposomes (1.5 μM), (4) Cou-6 liposomes (3 μM), (5) Ang2-Cou-6 liposomes (3 μM), (6) Cou-6 liposomes (6 μM), and (7) Ang2-Cou-6 liposomes (6 μM). (F) Quantitative analysis of fluorescence intensity. *, vs. Cou-6 liposomes; #, vs. 1.5 μM; ^, vs. 3 μM. $p < .05$; (G) analysis of cellular uptake of bEnd.3 cells treated with Cou-6 liposomes and Ang2-Cou-6 liposomes at a series of time points by flow cytometry; (a) blank control, (b) Cou-6 liposomes (1 h), (c) Ang2-Cou-6 liposomes (1 h), (d) Cou-6 liposomes (2 h), (e) Ang2-Cou-6 liposomes (2 h), (f) Cou-6 liposomes (4 h), and (g) Ang2-Cou-6 liposomes (4 h). (H) Quantitative analysis of fluorescence intensity. *, vs. Cou-6 liposomes; #, vs. 1 h; ^, vs. 2 h. $p < .05$. All data are presented as mean \pm SD ($n = 3$).

highest in the bEnd.3 cells, illustrating the enhanced targeting effect enabled by the Ang2 modification. This may be mainly related to the endocytosis mediated by the binding of Ang2 to LRP receptors on bEnd.3 cells (Song et al., 2021).

3.3. Transport across the BBB model *in vitro*

BBB model *in vitro* has been applied in our previous studies, and it was proved that the requirements of BBB model *in vitro* were met (Kong et al., 2020). First, the intracellular distribution of N2a cells in the co-cultured BBB model was observed by fluorescence microscope. The results showed that the fluorescence of Ang2-Cou-6 liposomes was higher

than that of Cou-6 liposomes (Figure 3(A,B), $p < .05$). In addition, the fluorescence signal in N2a cells was quantitatively analyzed by flow cytometry in order to more accurately analyze the ability of liposomal formulations to cross BBB *in vitro*, as shown in Figure 3(C,D). Similarly, the higher fluorescence intensity was found in N2a cells from the Ang2-Cou-6 liposomes group, and was significantly higher than that from the Cou-6 liposomes group ($p < .05$). Therefore, we believe that Ang2 modified liposomes may be used as a carrier to transport anti-AD drugs through BBB. However, the protective effect of Ang2-ICA/TSIIA liposomes on nerve cells of AD model has not been demonstrated in this study, and will be further explored in subsequent studies.

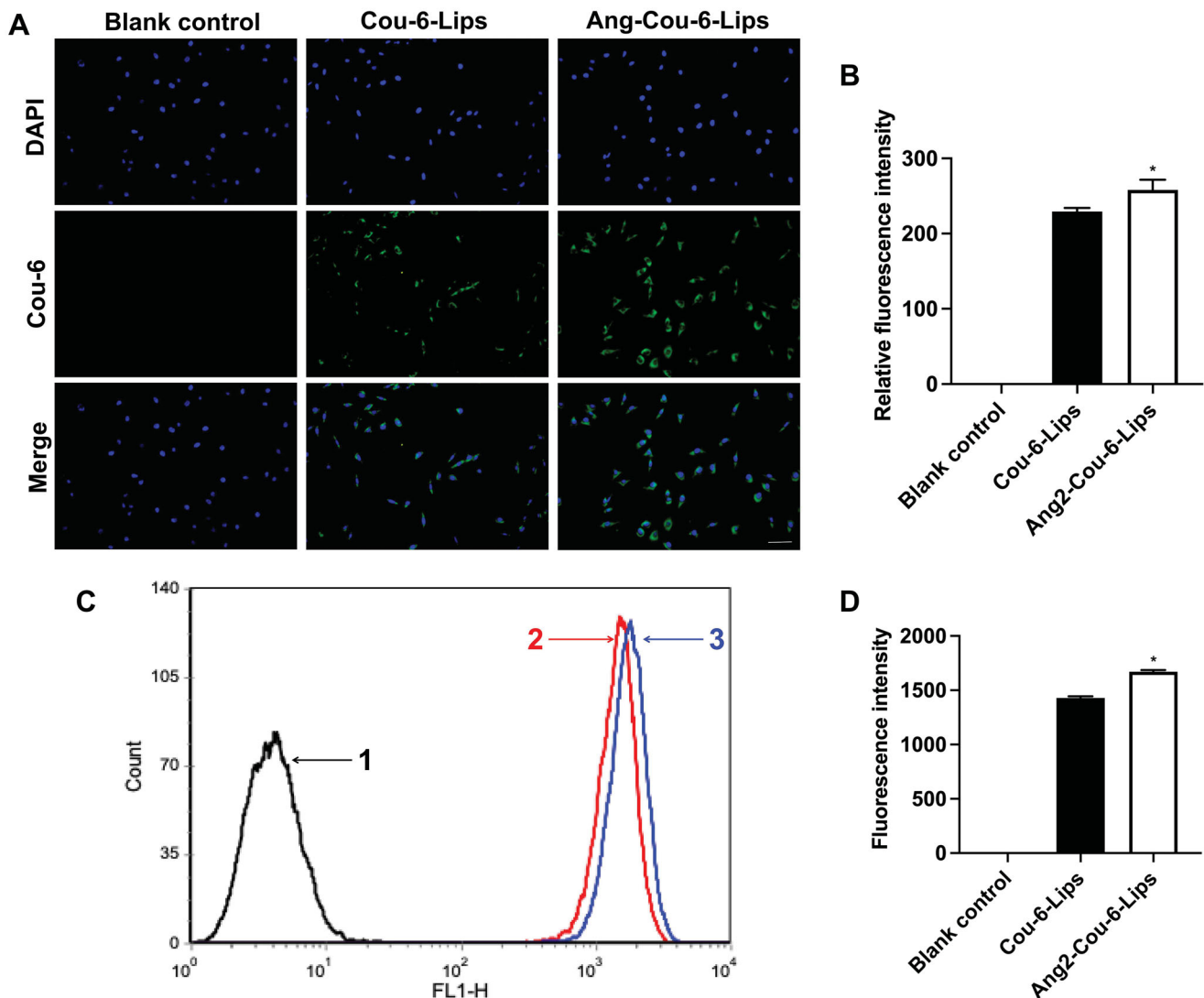


Figure 3. The capability of liposomal formulations to across BBB *in vitro*. (A) Fluorescent signals within N2a cells are observed through a microscope, scale bar = 50 μm ; (B) semi-quantitative analysis of relative fluorescence intensity. *, vs. Cou-6 liposomes. $p < .05$; (C) fluorescence intensity was analyzed by flow cytometry; (D) quantitative analysis of fluorescence intensity. *, vs. Cou-6 liposomes. $p < .05$. All data are presented as mean \pm SD ($n = 3$).

3.4. Imaging of liposomes in APP/PS-1 mice

To observe the brain-targeting capacity of Ang2 modified liposomes in APP/PS1 mice, ICA/TSIIA was substituted for DiR fluorescent dye, a dye commonly used as a fluorescent marker *in vivo*. The results exhibited that application of DiR liposomes and Ang2 modified DiR liposomes resulted in brain-targeting effects in APP/PS1 mice. Figure 4(A) shows representative images of APP/PS1 mice after tail vein injection of a various of liposomal formulations. The results showed that appropriate fluorescence signals were observed in the brain after the administration of DiR liposomes during 0–12 h, and little fluorescence signals could be found at 24 h. In the Ang2 modified DiR liposomes group, a strong fluorescence signal was observed in the brain and maintained for 24 h. APP/PS1 mice, which are of the C57BL/6 strain, were used in this study, and the fluorescence signal may be interfered by the hair of the mice. Therefore, the fluorescence signal of tissues and organs *in vivo* was analyzed. Figure 4(B) shows optical images of major organs *in vivo* after

APP/PS1 mice were sacrificed at 24 h. The results showed that the fluorescence signal was still observed in brain tissue, liver, and spleen. Similarly, the fluorescence signal of Ang2-DiR liposomes was significantly stronger than that of DiR liposomes in brain tissue, suggesting that the modification of Ang2 on liposome surface endowed it with brain targeting capacity. The prolonged circulation time and the enhancement of brain accumulation of liposomes *in vivo* were related to the addition of the hydrophilic long circulation material DSPE-PEG₂₀₀₀ and modification of the active targeting molecule Ang2 to liposomes (Li et al., 2019). Studies have shown that LRP1 has the potential to act as a specific receptor for brain-targeting molecules in AD models. The modification of Ang2 on the surface of pegylated gold nanoparticles can increase the cell penetration ability of bend.3, and increased the content of gold nanoparticles in brain tissue *in vivo* (Morales-Zavala et al., 2017). In addition, the modification of Ang2 on lipid nanocomposites can significantly increase intracranial drug delivery in AD mice, and the above study confirmed that Ang2 modified nanodrug carrier has good

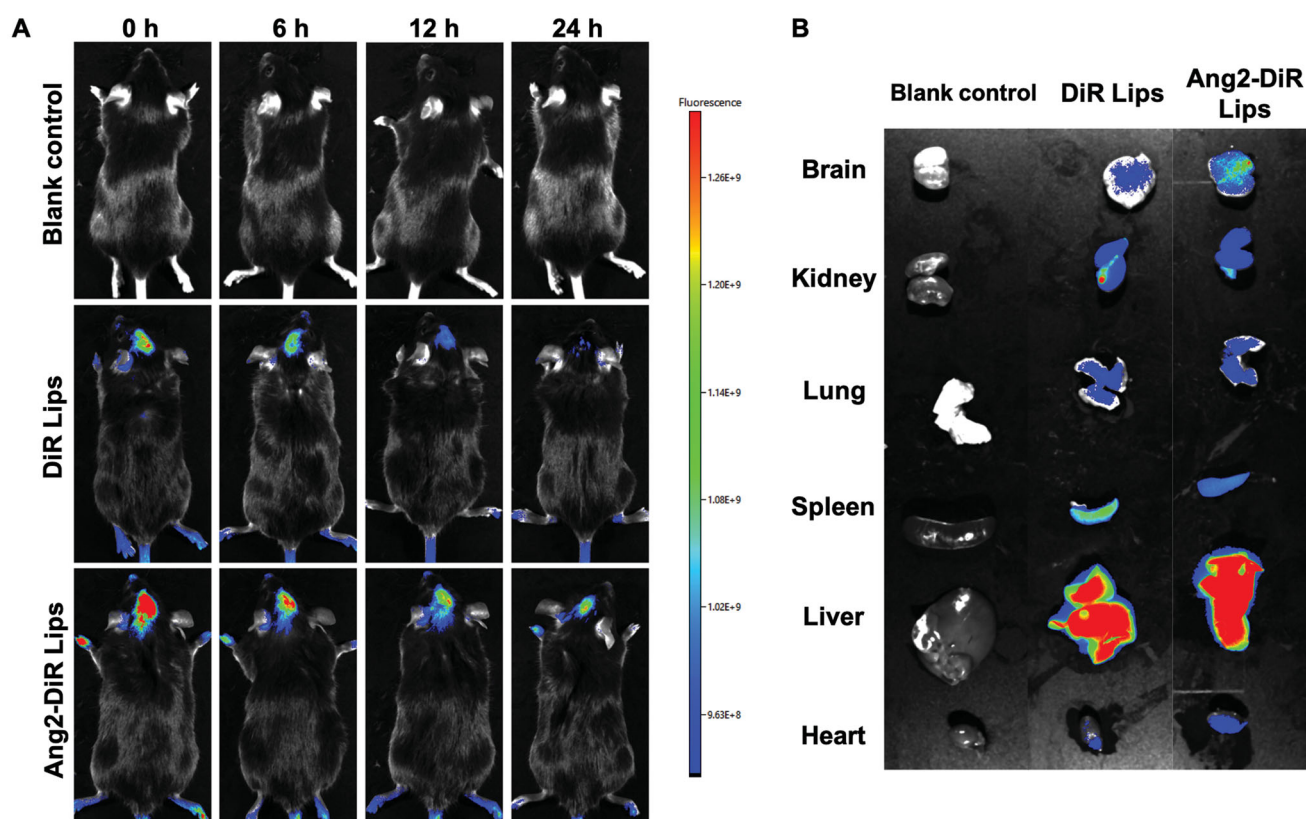


Figure 4. Real-time imaging observation after intravenous administration of varying liposomal formulations in APP/PS-1 mice. (A) Real-time images *in vivo*; (B) *ex vivo* optical images of brain, heart, liver, spleen, lung, and kidney tissues at 24 h ($n = 3$).

brain targeting ability (Han et al., 2022). In this study, our results also confirm the above views.

3.5. The protective effect of Ang2-ICA/TSIIA liposomes *in vivo*

3.5.1. Ang2-ICA/TSIIA liposomes improved cognitive function and $A\beta$ deposition in APP/PS1 mice

AD, the most common cause of dementia, is characterized by onset, progressive mental decline, and personality and emotional disorders. The pathogenesis of AD is not fully understood. As toxic protein, $A\beta$ plays an adverse role in the pathogenesis of AD (Panza et al., 2019). $A\beta$ oligomers affect cytoskeletal changes and the fate of nerve cells, leading to neuronal loss and thereby impaired memory and cognitive function (Liu et al., 2018a). Therefore, in the present study, free ICA/TSIIA, ICA/TSIIA liposomes and Ang2-ICA/TSIIA liposomes were used to treat APP/PS1 mice, respectively, and was used to evaluate the learning and memory ability of APP/PS1 mice were evaluated by Morris water maze after treatment with a various of formulations. During the navigation test, untreated APP/PS1 mice showed severe learning and memory deficits, while the mice treated with various formulations revealed learning and memory abilities significantly improved (Figure 5(A–D), $p < .05$). By comparison, APP/PS1 mice treated with Ang2-ICA/TSIIA liposomes performed significantly better than free ICA/TSIIA and ICA/TSIIA liposomes. Nesting behavior that has been used to evaluate the cognitive abilities of AD Tg mice is assessed here. After

the mice were treated, the mice of Ang2-ICA/TSIIA liposomes group had the highest nesting scores, followed by ICA/TSIIA liposomes and free ICA/TSIIA (Figure 5(E,F)). Next, we observed strong $A\beta$ plaque deposits in the cerebral cortex and hippocampus of APP/PS1 mice using immunohistochemical staining. After treatment with various drug formulations, APP/PS1 mice showed a significant reduction in amyloid deposition in the brain, with the most significant reduction in the Ang2-ICA/TSIIA liposomes group (Figure 6(A), $p < .05$). In addition, the expression of $A\beta_{1-42}$ protein was analysis by western blot, and it was found that the expression of $A\beta_{1-42}$ protein decreased after treatment with various formulations ($p < .05$). Similarly, the decrease of $A\beta_{1-42}$ protein was most obvious in Ang2-ICA/TSIIA liposomes group (Figure 6(B,C)). These results suggest that Ang2-ICA/TSIIA liposomes have the strongest effect on improving learning and memory ability and inhibiting $A\beta_{1-42}$ plaque deposition in APP/PS1 mice.

3.5.2. Ang2-ICA/TSIIA liposomes inhibited oxidative stress in APP/PS1 mice

Oxidative stress is considered to be one of the potential triggers for the onset of AD, a state in which the antioxidant defense levels are out of balance with free radicals, which induces potential brain damage (Tönnies & Trushina, 2017). There is evidence that oxidative stress occurs prior to the appearances of senile plaques and neurofibrillary tangles, which contributes to the progression of AD symptoms (Anwar et al., 2021). Glutathione peroxidase is an important antioxidant in the body, which can scavenge free radicals

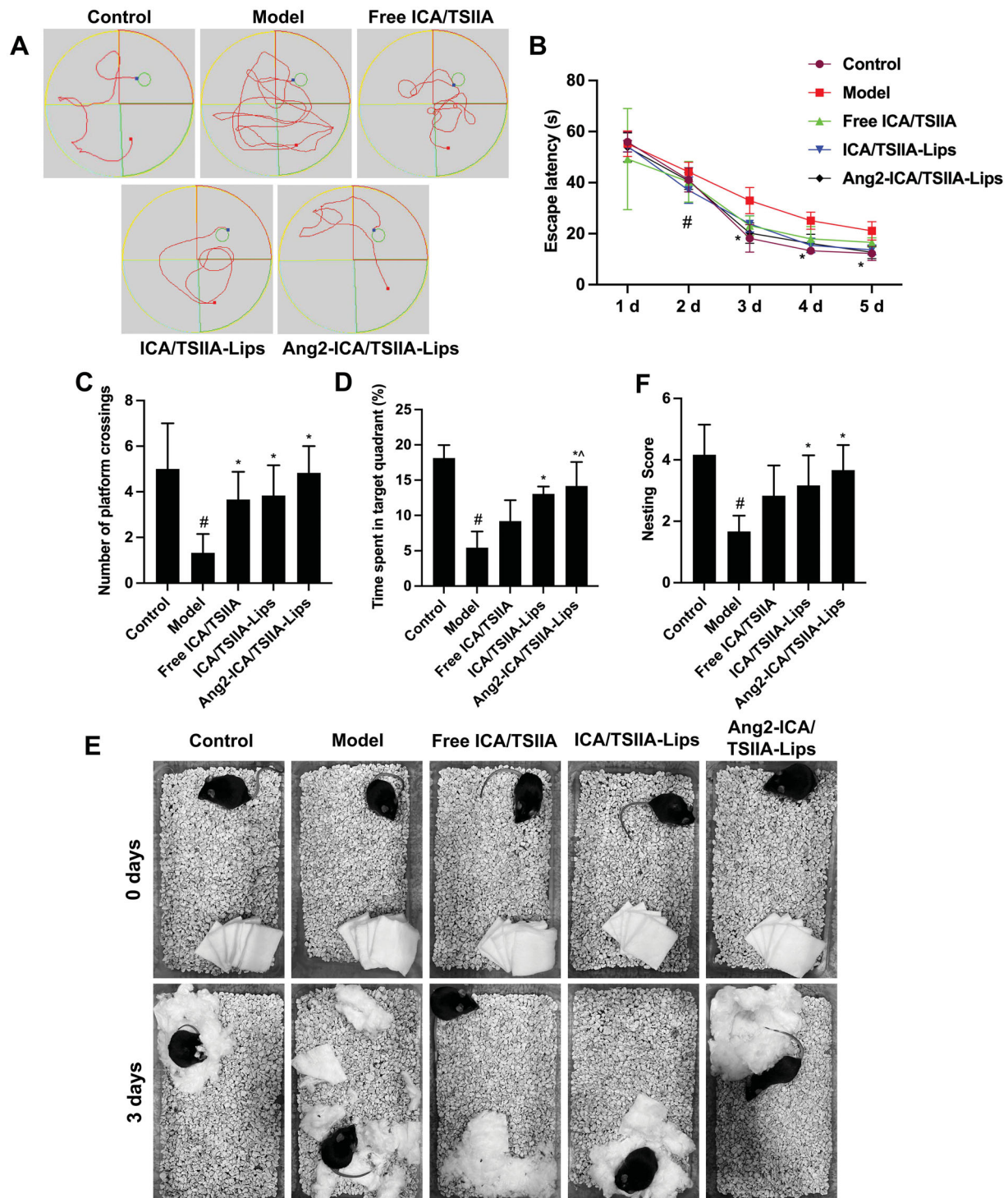


Figure 5. Improving effects of varying formulations on the cognitive decline of APP/PS1 mice. (A) The representative swimming paths in the water maze trial on day 5. (B) Escape latency of the water maze task. #, vs. control; *, vs. model. $p < .05$; (C) number of crossing the platform. #, vs. control; *, vs. model. $p < .05$; (D) the time spent of mice in the target quadrant. #, vs. control; *, vs. model; \wedge , vs. free ICA/TSIIA liposomes. $p < .05$; (E) representative images of nesting behavior in different groups of mice at 0 and 3 days. (F) Analysis of nesting score in APP/PS1 mice after treatment with the varying formulations. #, vs. control; *, vs. model. $p < .05$. All data are presented as mean \pm SD ($n = 6$).

and exert antioxidant effects, while MDA is a lipid metabolite, which is the main degradation product of lipid peroxidation, and it can be used as an indicator that brain tissue is attacked by free radicals (Wang et al., 2019). In addition, previous reports have shown a significant decrease in brain SOD levels in patients with AD, and increased SOD enzyme activity may be a therapeutic strategy to inhibit the progression

of AD. SOD combats the toxicity of oxygen radicals by catalyzing the reduction of superoxide radical anions into hydrogen peroxide (Gomaa et al., 2019). So that we analyzed the activity of PSH-Px (Figure 7(A)), SOD (Figure 7(B)), and MDA content (Figure 7(C)) in brain tissue to evaluate the ability of varying formulations against oxidative stress. We found that all drug treatment groups showed varying degrees of

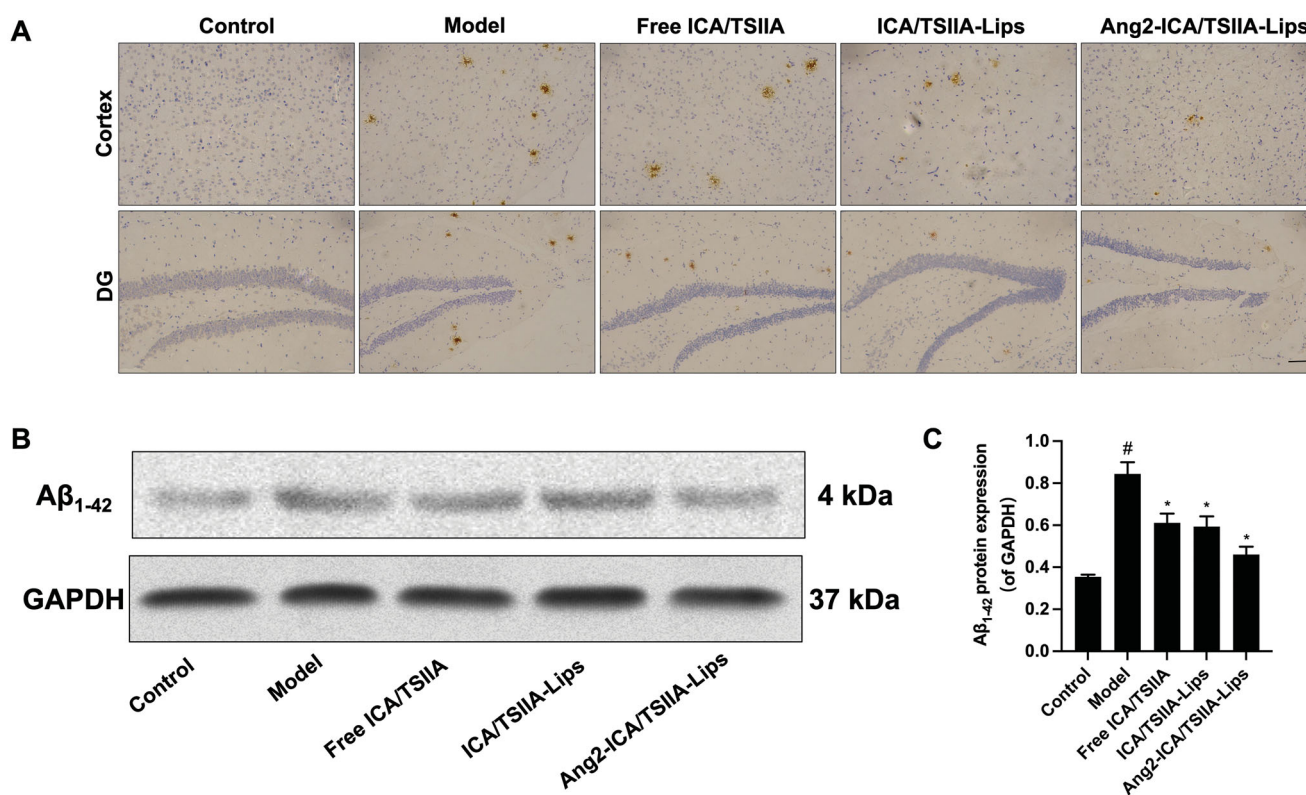


Figure 6. Reversal effect of varying formulations on Aβ deposition in APP/PS1 mice. (A) Representative images of Aβ₁₋₄₂ plaques in cortex and hippocampus by immunohistochemical staining, scale bar = 50 μm (n = 3); (B) the representative bands of Aβ₁₋₄₂ proteins; (C) semi-quantitative analysis of Aβ₁₋₄₂ proteins expression by densitometry after treatment with the varying formulations. Data are presented as mean ± SD (n = 3). #, vs. control; *, vs. model. *p* < .05.

improvement in oxidative stress compared to the model group (Figure 7(A–C)). Among them, Ang2-ICA/TSIIA liposomes have the strongest regulation effect on PSH-Px, SOD activity, and MDA content, followed by ICA/TSIIA liposomes (*p* < .05). These results revealed that Ang2-ICA/TSIIA liposomes enhanced the antioxidant stress capacity of ICA and TSIIA in the treatment of AD.

3.5.3. Ang2-ICA/TSIIA liposomes reduced neuroinflammation in APP/PS1 mice

Neuroinflammation plays a vital role in the pathological process of AD, which is mediated primarily by abnormal activation of immune cells in brain, and astrocytes and microglia are the cells in the brain that are primarily responsible for immune regulation. Aβ deposition can induce abnormal activation of glial cells. Hyper-activation of microglia not only leads to a weakening of the clearance effect on Aβ, but also exhibits a pro-inflammatory effect, and inflammatory factors such as IL-6, TNF-α, and IL-1β are released in large quantities (Lei et al., 2021). Astrocytes also show neurotoxic effects after activation, prompting increased release of inflammatory mediators, leading to neurodegeneration and synaptic loss, exacerbating cognitive impairment (Xu et al., 2014; Zhang et al., 2016). Hence, we examined the astrocyte marker GFAP and the microglia marker Iba-1 (Figure 7(D–E)), as well as IL-6, TNF-α, and IL-1β expression levels (Figure 7(F–H)). We found that since both ICA and TSIIA have certain anti-inflammatory effects, all three formulations significantly attenuate

neuroinflammation, and the ability of Ang2-ICA/TSIIA liposomes is the most prominent (Figure 7(D–H), *p* < .05). These results suggest that Ang2-ICA/TSIIA liposomes play a neuroprotective role by inhibiting glial cell activation and inhibiting inflammatory cytokine production *in vivo*.

3.5.4. Ang2-ICA/TSIIA liposomes inhibited apoptosis in APP/PS1 mice

As we all know, Aβ₁₋₄₂ induces oxidative stress and neuroinflammation that results in DNA damage and caspase-dependent neuronal apoptosis, which plays a crucial part in neurodegeneration (Fang et al., 2018). Hence, alleviating the apoptosis may be a possible treatment for AD. The mitochondrial pathway is the main process of inducing apoptosis, mainly mediated by Bcl-2 family and caspase. The Bcl-2 family consists of pro-apoptotic proteins (Bax, Bad, and Bak) and anti-apoptotic proteins (Bcl-2 and Bcl-XL) (Pahrudin Arrozi et al., 2020). Bax can increase mitochondrial permeability, release pro-apoptotic factors, and inhibit anti-apoptotic Bcl-2 family proteins to trigger caspase signaling, leading to neuronal apoptosis (Lu et al., 2021). In order to evaluate the inhibitory effect of varying formulations on nerve cell apoptosis *in vivo*, the paraffin sections of brain tissue treated with free ICA/TSIIA, ICA/TSIIA liposomes or Ang2-ICA/TSIIA liposomes were stained by immunohistochemistry. The expression of Bax and caspase-3 was significantly increased, while Bcl-2 is not expressed or at a low level in the hippocampus and cortex of APP/PS1 mice. After Ang2-ICA/TSIIA liposomes

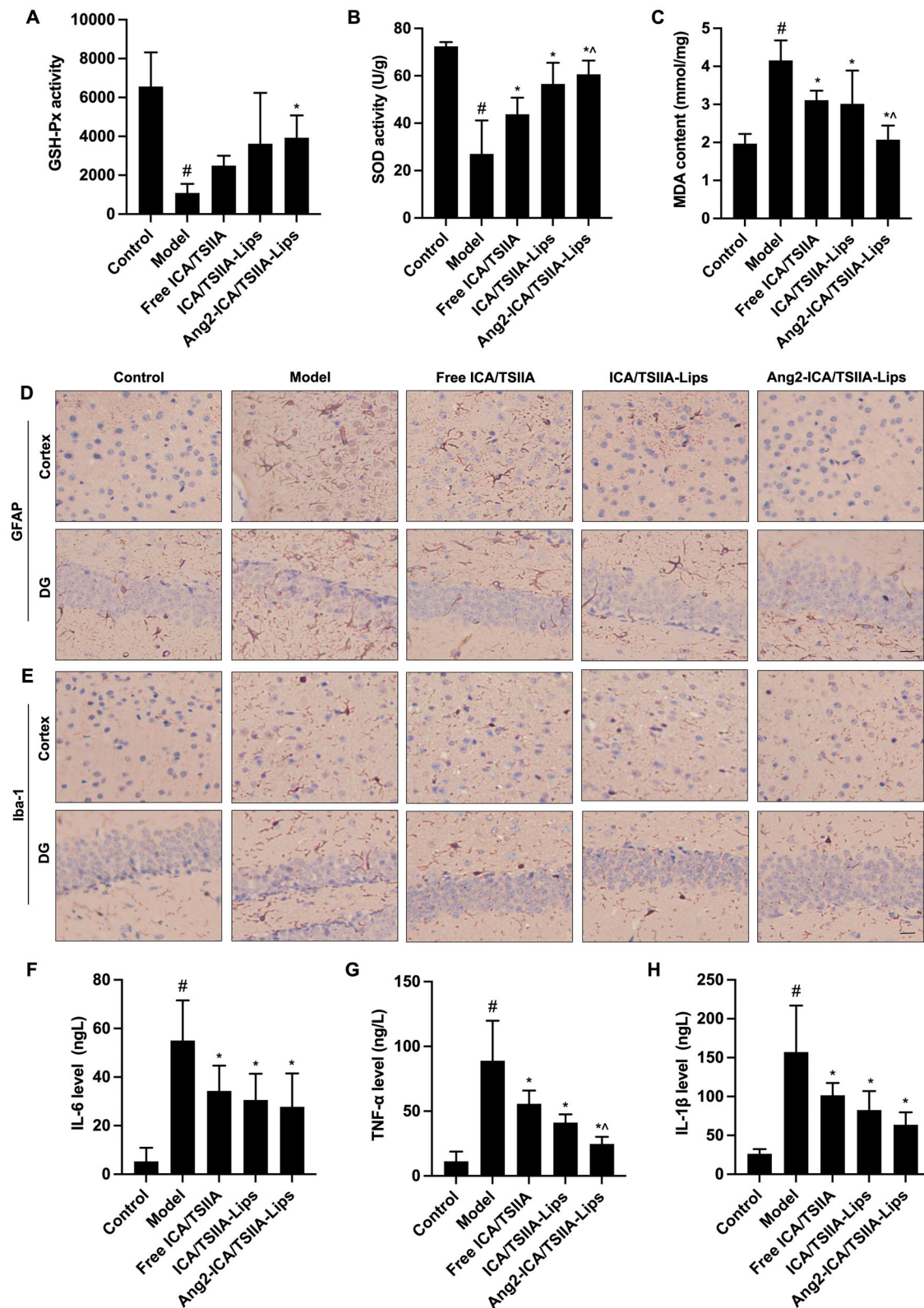


Figure 7. Inhibitory effect of varying formulations on oxidative stress and neuroinflammation in APP/PS1 mice. (A–C) Effect of the varying formulations on oxidative stress. The activity of GSH-Px (A), SOD (B), and the content of MDA (C) and in brain tissues detected. Data are presented as mean \pm SD ($n = 6$). #, vs. control; *, vs. model; ^, vs. free ICA/TSIIA liposomes; (D, E) effect of the varying formulations on neuroinflammation. Representative images of astrocytes (GFAP) (D) and microglia (Iba-1) (E) in cortex and hippocampus of APP/PS-1 mice by immunohistochemical staining, scale bar = 250 μ m ($n = 5$); (F–H) the levels of IL-6 (F), TNF- α (G), and IL-1 β (H) in brain tissues detected by ELISA. Data are presented as mean \pm SD ($n = 6$). #, vs. control; *, vs. model; ^, vs. free ICA/TSIIA liposomes.

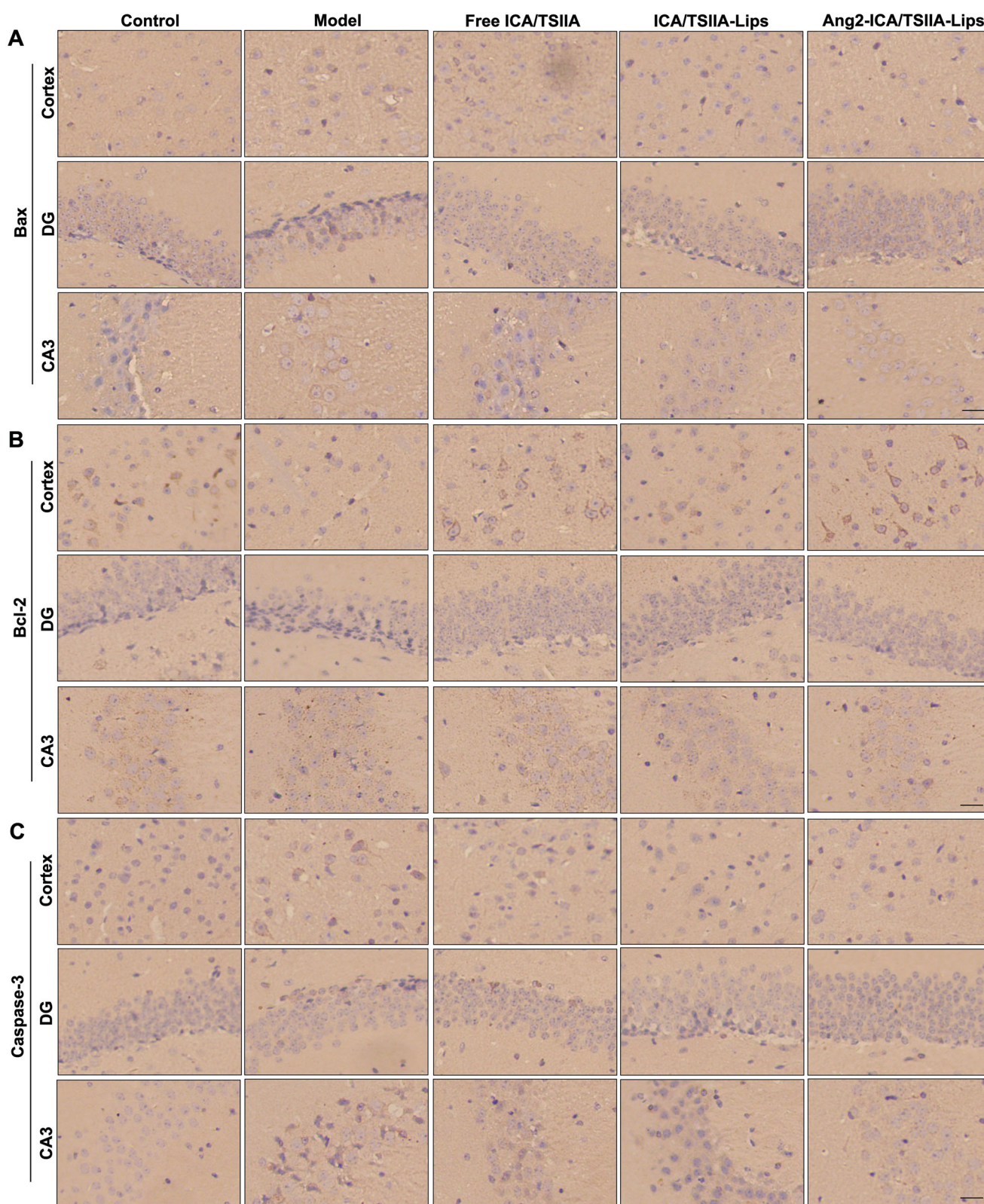


Figure 8. Inhibitory effect of varying formulations on apoptosis in APP/PS1 mice. (A–C) Representative images of apoptotic-related proteins Bax (A), Bcl-2 (B), and caspase-3 (C) in cortex and hippocampus of APP/PS-1 mice by immunohistochemical staining, scale bar = 250 μ m ($n = 5$).

treatment, the expression of Bax and caspase-3 was significantly decreased, while the expression of Bcl-2 was significantly increased (Figure 8(A–C)). These results indicated that Ang2-ICA/TSIIA liposomes could inhibit neuronal apoptosis in AD mice.

3.5.5. Ang2-ICA/TSIIA liposomes reversed neuronal damage in APP/PS1 mice

Neuronal damage and loss are the main causes of cognitive dysfunction in AD patients. In this study, the effects of varying formulation on the injury and loss of hippocampal and

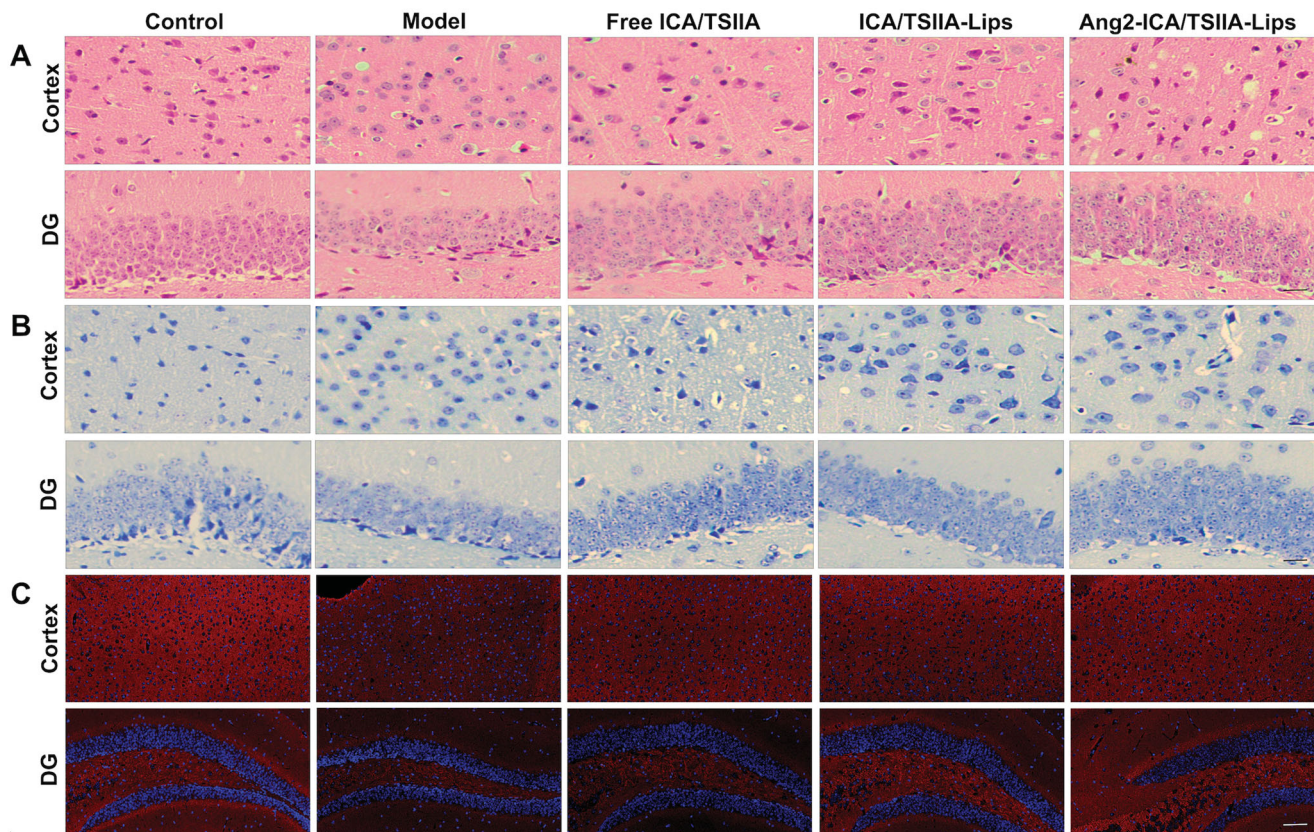


Figure 9. Improving effect of varying formulations on neuronal damage in APP/PS1 mice. (A) Representative images of HE staining of the cortex and hippocampus of APP/PS1 mice, scale bar = 250 μm ($n = 6$); (B) representative images of Nissl staining of the cortex and hippocampus of APP/PS1 mice, scale bar = 250 μm ($n = 6$); (C) representative images of SYN in cortex and hippocampus of APP/PS-1 mice by immunofluorescence staining, scale bar = 50 μm ($n = 6$).

cortical neurons in APP/PS1 mice were observed by HE staining and Nissl staining (Zhang et al., 2021). HE staining showed that the neurons in the blank control group were intact and neatly arranged, while the neurons in the hippocampus and cortex of APP/PS1 mice were in an unhealthy state with disordered arrangement, dark staining, atrophy, or even disappearance of neurons. Compared with the model group, free ICA/TSIIA, ICA/TSIIA liposomes, or Ang2-ICA/TSIIA liposomes treatment reduced the damage of hippocampal and cortical neurons, with normal morphology, orderly and complete arrangement of neurons (Figure 9(A)). In APP/PS1 mice, Nissl bodies were significantly reduced and morphologically atrophied in hippocampal and cortical neurons. With the treatment of free ICA/TSIIA, ICA/TSIIA liposomes, or Ang2-ICA/TSIIA liposomes, the damage of Nissl bodies improved. Among them, Ang2-ICA/TSIIA liposomes showed the strongest ability to improve neuron damage and loss (Figure 9(B)). In addition, we observed the expression of synapse associated protein synaptophysin (SYN) by immunofluorescence staining, and its expression level can reflect the state of neuronal function (Liu et al., 2018b). The results showed that the expression of SYN in the hippocampus of mice in the model group was minimal, while the expression of SYN in the hippocampus of mice was increased after Ang2-ICA/TSIIA liposomes treatment, which further indicated that Ang2-ICA/TSIIA liposomes could reverse neuronal damage in APP/PS1 mice (Figure 9(C)). Based on these results, we can conclude that Ang2-ICA/TSIIA liposomes are a targeted

formulation with potential protective effect on neurons of AD model.

4. Conclusions

Overall, Ang2-ICA/TSIIA liposomes were successfully constructed, overcoming the poor water solubility of ICA and TSIIA. Ang2 modified on the surface of the liposomes as brain-targeted ligands is evaluated by cell uptake, trans-BBB evaluation *in vitro*, and optical imaging *in vivo* to evaluate the brain targeting efficiency of liposomes. They can transport liposomes throughout the BBB, exhibit brain targeting, and are able to cross the BBB. In addition, Ang2-ICA/TSIIA liposomes exert excellent anti-AD capabilities, including inhibiting $\text{A}\beta$ deposition, reducing oxidative stress and neuroinflammation, reducing nerve cell apoptosis, reversing neuronal damage and loss, and improving cognitive function. There is some controversy about Ang2 as a brain-targeted ligand in the AD model because its receptor LRP1 is expressed at a reduced level in the brain of AD (Storck & Pietrzik, 2017). LRP1 plays a vital role in the pathological process of AD. The BBB plays an important role in the mechanism of transporting clearance of $\text{A}\beta$ in AD, and LRP1 is a key receptor for the BBB to transport $\text{A}\beta$, and one of its functions in the brain endothelium is to transport $\text{A}\beta$ from brain tissue to blood circulation, thus playing a role in clearing $\text{A}\beta$ in the brain (Zhou et al., 2021). Moreover, the recently reports suggested that TSIIA was able to improve protein expression of

glucose transporter 1 (GLUT1) and LRP1, thereby improving pathological progression in AD mice (Ma et al., 2022). We believe that TSIIA encapsulated in liposomes can contribute to the recognition of LRP1 and Ang2. Although, experimentally, this approach would be able to deliver drugs to the brain of neurodegenerative diseases such as AD. However, there are few studies on cellular transport processes and human efficacy. Therefore, further researches are needed to fully understand the potential of LRP1 as a receptor-mediated therapeutic target for brain delivery.

Disclosure statement

The authors report no conflicts of interest in this work.

Funding

This work was supported by the China Medical Education Association's "Major Scientific Research Projects and Medical Technology Problems in 2020" program [Grant No. 2020KTS004], the Open fund of Key Laboratory of Ministry of Education for TCM Viscera-State Theory and Applications, Liaoning University of Traditional Chinese Medicine [No. zyx2102], the National Natural Science Foundation of China [Grant No. 81874347], the Liaoning Natural Science Foundation [Grant No. 2019-MS-226], and Natural Science Foundation of Huai'an city [No. HAB201915].

References

- Anwar F, Saleem U, Rehman AU, et al. (2021). Toxicity evaluation of the naphthalen-2-yl 3,5-dinitrobenzoate: a drug candidate for Alzheimer disease. *Front Pharmacol* 1:1.
- Baranowska-Wójcik E, Szwajgier D. (2020). Alzheimer's disease: review of current nanotechnological therapeutic strategies. *Expert Rev Neurother* 20:271–9.
- Cai N, Chen J, Bi D, et al. (2020). Specific degradation of endogenous tau protein and inhibition of tau fibrillation by tanshinone IIA through the ubiquitin–proteasome pathway. *J Agric Food Chem* 68:2054–62.
- Candela P, Saint-Pol J, Kuntz M, et al. (2015). In vitro discrimination of the role of LRP1 at the BBB cellular level: focus on brain capillary endothelial cells and brain pericytes. *Brain Res* 1594:15–26.
- Carita AC, Eloy JO, Chorilli M, et al. (2018). Recent advances and perspectives in liposomes for cutaneous drug delivery. *Curr Med Chem* 25:606–35.
- Chen C, Duan Z, Yuan Y, et al. (2017). Peptide-22 and cyclic RGD functionalized liposomes for glioma targeting drug delivery overcoming BBB and BBTB. *ACS Appl Mater Interfaces* 9:5864–73.
- Chen YJ, Zheng HY, Huang XX, et al. (2016). Neuroprotective effects of icariin on brain metabolism, mitochondrial functions, and cognition in triple-transgenic Alzheimer's disease mice. *CNS Neurosci Ther* 22:63–73.
- Dos Santos Rodrigues B, Lakkadwala S, Kanekiyo T, Singh J. (2020). Dual-modified liposome for targeted and enhanced gene delivery into mice brain. *J Pharmacol Exp Ther* 374:354–65.
- Duro-Castano A, Borrás C, Herranz-Pérez V, et al. (2021). Targeting Alzheimer's disease with multimodal polypeptide-based nanoconjugates. *Sci Adv* 7:eabf9180.
- Endo-Takahashi Y, Kurokawa R, Sato K, et al. (2021). Ternary complexes of pDNA, neuron-binding peptide, and PEGylated polyethyleneimine for brain delivery with nano-bubbles and ultrasound. *Pharmaceutics* 13:1003.
- Eratne D, Loi SM, Farrand S, et al. (2018). Alzheimer's disease: clinical update on epidemiology, pathophysiology and diagnosis. *Aust Psychiatry* 26:347–57.
- Fang XX, Sun GL, Zhou Y, et al. (2018). TGF- β 1 protection against A β 1-42-induced hippocampal neuronal inflammation and apoptosis by T β R-I. *Neuroreport* 29:141–6.
- Fornicola B, Cox A, Dal Magro R, et al. (2019). Nanomedicine for the treatment of Alzheimer's disease. *J Biomed Nanotechnol* 15:1997–2024.
- Gao H. (2016). Progress and perspectives on targeting nanoparticles for brain drug delivery. *Acta Pharm Sin B* 6:268–86.
- Geng L, Liu W, Chen Y. (2019). Tanshinone IIA attenuates A β -induced neurotoxicity by down-regulating COX-2 expression and PGE2 synthesis via inactivation of NF- κ B pathway in SH-SY5Y cells. *J Biol Res* 26:15.
- Gomaa AA, Makboul RM, El-Mokhtar MA, et al. (2019). Terpenoid-rich *Elettaria cardamomum* extract prevents Alzheimer-like alterations induced in diabetic rats via inhibition of GSK3 β activity, oxidative stress and pro-inflammatory cytokines. *Cytokine* 113:405–16.
- Han G, Bai K, Yang X, et al. (2022). "Drug-carrier" synergy therapy for amyloid- β clearance and inhibition of tau phosphorylation via biomimetic lipid nanocomposite assembly. *Adv Sci* e2106072.
- He C, Wang Z, Shi J. (2020). Pharmacological effects of icariin. *Adv Pharmacol* 87:179–203.
- Huang N, Li Y, Zhou Y, et al. (2019). Neuroprotective effect of tanshinone IIA-incubated mesenchymal stem cells on A β 25-35-induced neuroinflammation. *Behav Brain Res* 365:48–55.
- Kong L, Li XT, Ni YN, et al. (2020). Transferrin-modified osthole PEGylated liposomes travel the blood–brain barrier and mitigate Alzheimer's disease-related pathology in APP/PS-1 mice. *Int J Nanomedicine* 15:2841–58.
- Lakkadwala S, Dos Santos Rodrigues B, Sun C, Singh J. (2019). Dual functionalized liposomes for efficient co-delivery of anti-cancer chemotherapeutics for the treatment of glioblastoma. *J Control Release* 307:247–60.
- Lei T, Yang Z, Xia X, et al. (2021). A nanocleaner specifically penetrates the blood–brain barrier at lesions to clean toxic proteins and regulate inflammation in Alzheimer's disease. *Acta Pharm Sin B* 11:4032–44.
- Li F, Dong HX, Gong QH, et al. (2015). Icariin decreases both APP and A β levels and increases neurogenesis in the brain of Tg2576 mice. *Neuroscience* 304:29–35.
- Li S, Xu Q, Zhao L, et al. (2019). Angiopep-2 modified cationic lipid-poly-lactic-co-glycolic acid delivery temozolomide and DNA repair inhibitor Dba1 to achieve synergetic chemo-radiotherapy against glioma. *J Nanosci Nanotechnol* 19:7539–45.
- Liu SY, Lu S, Yu XL, et al. (2018a). Fruitless wolfberry-sprout extract rescued cognitive deficits and attenuated neuropathology in Alzheimer's disease transgenic mice. *Curr Alzheimer Res* 15:856–68.
- Liu Y, Zhang Y, Zheng X, et al. (2018b). Galantamine improves cognition, hippocampal inflammation, and synaptic plasticity impairments induced by lipopolysaccharide in mice. *J Neuroinflammation* 15:112.
- Lu BL, Li J, Zhou J, et al. (2016). Tanshinone IIA decreases the levels of inflammation induced by A β 1-42 in brain tissues of Alzheimer's disease model rats. *Neuroreport* 27:883–93.
- Lu S, Wei X, Zhang H, et al. (2021). Protective effect of 2-dodecyl-6-methoxycyclohexa-2, 5-diene-1, 4-dione, isolated from *Averrhoa carambola* L., against A β 1-42-induced apoptosis in SH-SY5Y cells by reversing Bcl-2/Bax ratio. *Psychopharmacology* 238:193–200.
- Ma D, Zhao L, Zhang L, et al. (2021). Icariin promotes survival, proliferation, and differentiation of neural stem cells in vitro and in a rat model of Alzheimer's disease. *Stem Cells Int* 2021:9974625.
- Ma HH, Wan C, Zhang LD, et al. (2022). Sodium tanshinone IIA sulfonate improves cognitive impairment via regulating A β transportation in AD transgenic mouse model. *Metab Brain Dis* 37:989–1001.
- Morales-Zavala F, Arriagada H, Hassan N, et al. (2017). Peptide multifunctionalized gold nanorods decrease toxicity of β -amyloid peptide in a *Caenorhabditis elegans* model of Alzheimer's disease. *Nanomedicine* 13:2341–50.
- Pahrudin Arrozi A, Shukri SNS, Wan Ngah WZ, et al. (2020). Comparative effects of alpha- and gamma-tocopherol on mitochondrial functions in Alzheimer's. *Sci Rep* 10:8962.

- Panza F, Lozupone M, Logroscino G, Imbimbo BP. (2019). A critical appraisal of amyloid- β -targeting therapies for Alzheimer disease. *Nat Rev Neurol* 15:73–88.
- Poovaiah N, Davoudi Z, Peng H, et al. (2018). Treatment of neurodegenerative disorders through the blood–brain barrier using nanocarriers. *Nanoscale* 10:16962–83.
- Ross C, Taylor M, Fullwood N, Allsop D. (2018). Liposome delivery systems for the treatment of Alzheimer's disease. *Int J Nanomedicine* 13: 8507–22.
- Ruan S, Zhou Y, Jiang X, Gao H. (2021). Rethinking CRITID procedure of brain targeting drug delivery: circulation, blood brain barrier recognition, intracellular transport, diseased cell targeting, internalization, and drug release. *Adv Sci* 8:2004025.
- Shah S, Dhawan V, Holm R, et al. (2020). Liposomes: advancements and innovation in the manufacturing process. *Adv Drug Deliv Rev* 154–155:102–22.
- Sheng C, Xu P, Zhou K, et al. (2017). Icarin attenuates synaptic and cognitive deficits in an A β 1-42-induced rat model of Alzheimer's disease. *Biomed Res Int* 2017:7464872.
- Song P, Song N, Li L, et al. (2021). Angiopep-2-modified carboxymethyl chitosan-based pH/reduction dual-stimuli-responsive nanogels for enhanced targeting glioblastoma. *Biomacromolecules* 22:2921–34.
- Storck SE, Pietrzik CU. (2017). Endothelial LRP1 – a potential target for the treatment of Alzheimer's disease: theme: drug discovery, development and delivery in Alzheimer's disease Guest Editor: Davide Brambilla. *Pharm Res* 34:2637–51.
- Tönnies E, Trushina E. (2017). Oxidative stress, synaptic dysfunction, and Alzheimer's disease. *J Alzheimers Dis* 57:1105–21.
- Wang X, Xiong Z, Liu Z, et al. (2018). Angiopep-2/IP10-EGFRvIIIscFv modified nanoparticles and CTL synergistically inhibit malignant glioblastoma. *Sci Rep* 8:12827.
- Wang Y, Wang Q, Li J, et al. (2019). Glutamine improves oxidative stress through the Wnt3a/ β -catenin signaling pathway in Alzheimer's disease in vitro and in vivo. *Biomed Res Int* 2019:4690280.
- Xu PX, Wang SW, Yu XL, et al. (2014). Rutin improves spatial memory in Alzheimer's disease transgenic mice by reducing A β oligomer level and attenuating oxidative stress and neuroinflammation. *Behav Brain Res* 264:173–80.
- Yu C, Liu H, Guo C, et al. (2022). Dextran sulfate-based MMP-2 enzyme-sensitive SR-A receptor targeting nanomicelles for the treatment of rheumatoid arthritis. *Drug Deliv* 29:454–65.
- Yu Y, Pang Z, Lu W, et al. (2012). Self-assembled polymersomes conjugated with lactoferrin as novel drug carrier for brain delivery. *Pharm Res* 29:83–96.
- Zhang H, Su Y, Sun Z, et al. (2021). Ginsenoside Rg1 alleviates A β deposition by inhibiting NADPH oxidase 2 activation in APP/PS1 mice. *J Ginseng Res* 45:665–75.
- Zhang Q, Wu HH, Wang Y, et al. (2016). Neural stem cell transplantation decreases neuroinflammation in a transgenic mouse model of Alzheimer's disease. *J Neurochem* 136:815–25.
- Zheng X, Shao X, Zhang C, et al. (2015). Intranasal H102 peptide-loaded liposomes for brain delivery to treat Alzheimer's disease. *Pharm Res* 32:3837–49.
- Zhou L, Poon CC, Wong KY, et al. (2020). Prenylflavonoid icaritin induces estrogen response element-independent estrogenic responses in a tissue-selective manner. *J Endocr Soc* 4:bvz025.
- Zhou R, Chen LL, Yang H, et al. (2021). Effect of high cholesterol regulation of LRP1 and RAGE on A β transport across the blood–brain barrier in Alzheimer's disease. *Curr Alzheimer Res* 18:428–42.
- Zhu J, Zhang Y, Chen X, et al. (2021). Angiopep-2 modified lipid-coated mesoporous silica nanoparticles for glioma targeting therapy overcoming BBB. *Biochem Biophys Res Commun* 534:902–7.
- Zu Y, Mu Y, Li Q, et al. (2019). Icaritin alleviates osteoarthritis by inhibiting NLRP3-mediated pyroptosis. *J Orthop Surg Res* 14:307.